Coupled and optimized properties of a hybrid system integrating electrochemical cycles with perovskite solar cell

Tianjun Liao[1, 2*], Chun Cheng[1], Yawen Dai[1], Qijiao He[1], Qidong Xu[1], Meng Ni[1*]

[1]Department of Building and Real Estate, The Hong Kong Polytechnic University, Hung Hom, Kowloon, Hong Kong, China

[2]Department of Physics and Energy, Chongqing University of Technology, Chongqing 400054, China

Summary

The low-grade waste heat generated by the perovskite solar cells (PSCs) during the photoelectric conversion process will increase the temperature and the efficiency of PSCs. In present work, the waste heat from PSC is recovered by integrating a series of thermally regenerative electrochemical cycles (TRECs) with PSC to achieve energy cascade utilization and improve solar energy utilization. Based on the theories of conservation laws, electrochemistry, and thermodynamics, the formulas for the overall power generation and efficiency of the coupled system are derived. Firstly, the performance characteristics of three special circuit states of open circuit of TRECs, open circuit of PSC, and series electrical circuit of PSC-TRECs are studied to determine the maximum efficiency and optimal conditions. Secondly, the optimum performances of PSC and TRECs that generate electricity independently are studied, and a maximum efficiency 24.9% is obtained by numerical simulation. The proposed coupled system offers a new route for recycling of PSC's low-grade thermal energy.

KEYWORDS: perovskite solar cell (PSC), thermally regenerative electrochemical cycles (TRECs), coupled system, performance analysis, low-grade heat recovery

[*]Corresponding authors: Email: liaotianjunxmu@hotmail.com (T.J. Liao)
Email: meng.ni@polyu.edu.hk; Tel: 852-27664152; Fax: 852-27645131 (M. Ni)

Nomenclature

A_p area (m^2)
a absorption coefficient (m^{-1})
C_p specific heat capacity ($eV \cdot kg^{-1} \cdot K^{-1}$)
C_q specific charge capacity ($A \cdot s^{-1} \cdot kg^{-1}$)
c speed of light ($m \cdot s^{-1}$)
d thickness of perovskite material (nm)
E photon energy (eV)
E_g bandgap (eV)
G solar irradiance ($W \cdot m^{-2}$)
q charge of a positive electron (C)
h Planck constant ($eV \cdot s$)
I electrical current (A)
J_p operating current density of PSC ($A \cdot m^{-2}$)
J_{ph} photocurrent density ($A \cdot m^{-2}$)
J_0 reverse saturation current density ($A \cdot m^{-2}$)
k_B Boltzmann constant ($eV \cdot K^{-1}$)
m number of the cells charged simultaneously
N_i intrinsic concentration (m^{-3})
N_c conduction state density (m^{-3})
N_v valence band state density (m^{-3})
n number of TREC series
P power output (W)
Q heat flow (W)
r_s series internal resistance ($\Omega \cdot m^2$)
r_{sh} shunt resistance ($\Omega \cdot m^2$)
R_I internal resistance of TREC (Ω)
R_{L1} load resistance of PSC (Ω)
R_{L2} load resistance of TREC (Ω)
S entropy ($eV \cdot K^{-1}$)
ϕ spectral irradiation intensity ($W \cdot m^{-2} \cdot nm^{-1}$)
T temperature (K)

Greek symbols

α Isothermal temperature coefficient ($V \cdot K^{-1}$)
ε electromotive force (V)
κ_s extinction coefficient
λ wavelength of sunlight (m)
γ_{Auger} Auger recombination coefficient $\left(m^6 \cdot s^{-1} \right)$
τ_{SRH} SRH recombination time (μs)
η efficiency

Subscript

Auger Auger non-radiative recombination
E environment
OC open-circuit
P perovskite solar cell
r reverse saturation
R regenerative
SC short-circuit
SRH Shockley-Read-Hall non-radiative recombination
T thermally regenerative electrochemical cycles
H hot side
I internal resistance
i intrinsic
L cold side
max maximum
min minimum
M overall maximum point

Abbreviations

ETL electron transport layer
HTL hole transport layer
NRLs non-radiative recombination losses
PCE photo-generated carrier efficiency
OCV open-circuit voltage
PSC perovskite solar cell
PCBM phenyl-C61-butyric acid methyl ester
PEDOT: PSS poly (3, 4-ethylenedioxythiophene) polystyrene sulfonate
SRH Shockley-Read-Hall
TEM thermoelectric module
TREC thermally regenerative electrochemical cycle

1 | INTRODUCTION

Energy is the driving force for sustainable development. As one of the key energy technologies, solar cells can convert sunlight into electricity by means of the p-n junction's photovoltaic effect, which is an important approach for humans to alleviate and solve the problem of excessive consumption of traditional fossil energy and the associated environmental pollution.[1] Although the traditional silicon-based photovoltaic cells have been developed for many years, the high-cost and the complexity of silicon material purification and device preparation processes limit the commercialization process.[2] Therefore, the innovative development of alternative solar cells such as organic solar cells (OSCs), perovskite solar cells (PSCs), and dye-sensitized solar cells are of great significance for solving the energy crisis.[2,3] Due to the high absorption coefficient and extinction coefficient in perovskite material, the PSCs have important application prospects in the field of photoelectric conversion devices.[3] However, the previous works demonstrated that the irreversible thermal losses generated in the carriers of generation, radiative recombination, non-radiative recombination, and transport lead to the increase of the temperature.[4,5] The PSC releases low-grade waste heat into the environment through convective heat transfer.[6] In order to utilize the low-grade waste heat from PSC, the coupled systems integrating a thermoelectric module (TEM) with the PSC have been proposed and evaluated.[7-12] The maximum efficiency and the parametric optimal analysis of the PSC-TEM coupled system are presented. The results can offer some theoretical strategies for the design of a low-grade coupled energy cascade utilization system. Recently, the researchers proposed a new strategy for the solar cells waste heat recovery through thermally regenerative electrochemical cycles (TRECs).[13-15] The TRECs utilize electrochemical cells to charge at a high temperature and discharge at a low temperature, the charging voltage is smaller than the discharge voltage, and then generate power through the net output

voltage.[16-20] The thermal-to-electricity conversion efficiency of 5.7% is achievable by TREC at a temperature difference of 50 ℃ for charge and discharge.[17] The reported works demonstrated that TREC can exhibit higher performance as it is driven by solar energy and fuel cells.[21-23] Cheng *et. al.*[24] introduced mixed membranes with mixed pH electrolytes to design a high-performance TREC with Zn anode and NiHCF cathode under a temperature difference of 30 °C, achieving a high thermopower coefficient of −2.270 $mV \cdot K^{-1}$. The established thermodynamic model and obtained results are helpful for recovery the low-grade waste heat in PSC. However, there are no literatures on the PSCs' waste heat recovery based on TRECs. It is still unknown to what extent the use of TRECs can help recover the waste heat from PSC and under what conditions the overall performance can be maximized. The investigation on the above-mentioned problem is significant for the efficient utilization of solar energy. Recently, Xu *et. al.* [25] proposed a simulation equivalent circuit model describing the volt-ampere characteristics of the PSCs, in which the photon cycling, light trapping structure, bulk recombination and surface recombination, and series-parallel resistance loss are considered. By comparing the simulation curve and the experimental curve, it was verified that the equivalent circuit model can accurately describe the PSCs's electrical performance.

In this paper, the PSC's equivalent circuit model and TREC's thermodynamic-electrochemistry model are applied to construct a PSC-TRECs coupled system for energy utilization enhancement. Based on the PSC's equivalent circuit model and the TRECs' thermodynamic-electrochemistry model, the expressions for the overall electricity generation and efficiency of the coupled system are theoretically derived. The optimum performances and the parametric analysis are provided. The effects of the non-radiative recombination and the PSC's front surface on the optimum performances and the operating conditions are revealed.

2 | MODEL DESCRIPTION AND WORKING PRINCIPLE

The conceptual diagrams of a PSC-TREC coupled system, TREC's temperature (*T*)-entropy (*S*) cycle, and two equivalent electrical circuits of the PSC and the TREC are depicted in Fig. 1. In Fig. 1(a), A_{p} stands for the front surface area of the PSC's electrode, and G denotes the solar irradiance. The hole transport layer (HTL) and electron transport layer (ETL) locate at the top and the bottom of the perovskite active layer. The PEDOT: PSS [poly (3, 4-ethylenedioxythiophene) polystyrene sulfonate] and PCBM (phenyl-C61-butyric acid methyl ester) are chosen to design the HTL and the ETL.[24] The indium tin oxide (ITO) coated with glass works as an optical transparent electrode. The back electrode is placed at the bottom of the ETL. Electrons and holes are excited as sunlight is absorbed by the perovskite layer. Under the built-in electric field, the electrons and the holes transport to the ETL and the HTL by means of diffusion and drifting. In order to increase the operating voltage, n TRECs are connected in series to form an electrochemical subsystem, in which the top and the bottom are contacted with the back surface of the PSC and the environment by the conduction materials. The waste heat generated by the PSC drives the TRECs to absorb and release heat flows Q_{H} and Q_{L} through electrochemical reactions. Fig. 1(b) depicts a schematic diagram of temperature (*T*)-entropy (*S*) cycle, which consists of heating, charging, cooling, and discharging four processes.[22] After the process of preheating, the TREC enters the charging process and absorbs heat flow Q_{H} from the PSC. After the process of cooling, the TREC enters the discharging process and releases heat flow Q_{L} into the environment. Due to the non-ideal thermodynamic cycle, there exists regenerative loss during regeneration process.[13-15] Fig. 1(c) gives the equivalent electrical circuit of a PSC. The PSC's shunt resistance $r_{\mathrm{sh}} = 1.2\,\Omega\cdot\mathrm{m}^2$ and the series internal resistance $r_{\mathrm{s}} = 9\times10^{-4}\,\Omega\cdot\mathrm{m}^2$ are chosen from Ref.

[26]. The sunlight drives the PSC excite the photocurrent density J_{ph}, and the reverse saturation current density J_r. When the circuit is connected to the load R_{L1}, the operating voltage V_P and the current density J_P and will be generated. Fig. 1(d) displays the equivalent electrical circuit of a TREC. ε_T and R_I are TREC's electromotive force and internal resistance.[14] When the circuit is connected to the load resistance R_{L2}, the operating voltage V_T and electrical current I_T and will be generated.[14]

The assumptions for the whole system are listed as follows:

(1) The temperatures T_H and T_L of the TRECs are considered to equal to those of the PSC and the environment, i.e., $T_H = T_P$ and $T_L = T_E$.

(2) The ideality in equivalent electrical circuit of a PSC is equal to 1.

(3) The PSC releases waste heat via convective heat transfer.

(4) The PSC's photon absorption coefficient is independent of the operating temperature T_P.

(5) The Bose-Einstein distribution $1/\left\{\exp\left[hc/\left(\lambda k_B T\right)\right]-1\right\}$ of the photons is simplified to Maxwell-Boltzmann distribution $1/\exp\left[hc/\left(\lambda k_B T\right)\right]$, where λ is the wavelength, k_B is the Boltzmann's constant, h means the Planck's constant.

2.1 | The electricity generation from a PSC

The PSC's equivalent electrical circuit can be described by a single diode model, as depicted in Fig. 1(c). The constraint equation for voltage and current density of a PSC is denoted as:[27-30]

$$J_P = J_{ph} - J_r - J_{sh} = J_{ph} - \left\{ J_{01} \exp\left[\frac{q\left(J_P r_s + V_P\right)}{k_B T_P} \right] - J_{02} \right\} - \frac{V_P + J_P r_s}{r_{sh}}, \quad (1)$$

where q is the charge of a positive electron.

The key current densities J_{ph} at the solar spectrum $\phi(\lambda)$, J_{01} at operating temperature T_P, and J_{02} at operating temperature T_E can be given by[30]

$$J_{\mathrm{ph}} = q\int_0^{\lambda_{\mathrm{g}}} \left\{1-\exp\left[-2a(\lambda)d\right]\right\}\phi(\lambda)PCE(\lambda)\frac{\lambda}{hc}d\lambda, \tag{2}$$

$$J_{01} = q\int_0^{\lambda_{\mathrm{g}}} \frac{2\pi hc^2}{\lambda^5}\frac{1-\exp\left[-2a(\lambda)d\right]}{\exp\left[hc/(\lambda k_{\mathrm{B}}T_{\mathrm{P}})\right]}d\lambda, \tag{3}$$

and

$$J_{02} = q\int_0^{\lambda_{\mathrm{g}}} \frac{2\pi hc^2}{\lambda^5}\frac{1-\exp\left[-2a(\lambda)d\right]}{\exp\left[hc/(\lambda k_{\mathrm{B}}T_{\mathrm{E}})\right]}d\lambda, \tag{4}$$

where T_{E} is the environment temperature. $a(\lambda)=4\pi/\lambda\kappa_{\mathrm{s}}$ accounts for the absorption coefficient. κ_{s} is the extinction coefficient [30]. d is the PSC's thickness. $PCE(\lambda)$ is the photo-generated carrier efficiency [30]. $\phi(\lambda)$ denotes the solar radiation spectrum at illumination AM 1.5G. c describes the vacuum speed of light. $\lambda_{\mathrm{g}}=hc/E_{\mathrm{g}}$ represents the wavelength corresponding the band-gap $E_{\mathrm{g}}=1.55\,\mathrm{eV}$. Based on Eqs. (1)-(4), the PSC's power production P_{PSC} is represented as

$$P_{\mathrm{PSC}} = V_{\mathrm{P}}J_{\mathrm{P}}A_{\mathrm{P}} = V_{\mathrm{P}}A_{\mathrm{P}}\left\{J_{\mathrm{ph}} - J_0\left[\exp\left(\frac{J_{\mathrm{P}}r_{\mathrm{s}}+V_{\mathrm{P}}}{k_{\mathrm{B}}T_{\mathrm{P}}/q}\right)-1\right]-\frac{V_{\mathrm{P}}+J_{\mathrm{P}}r_{\mathrm{s}}}{r_{\mathrm{sh}}}\right\}. \tag{5}$$

2.2 | Power production of TRECs

An electrochemical system using solid copper hexacyanoferrate (CuHCF) and Cu/Cu^{2+} as highly reversible electrode material for positive and negative electrodes in an aqueous electrolyte is chosen to recycle the PSC's low-grade heat, where the electrode materials have high capacity, low specific heat, and moderate temperature coefficient. Note that a single TREC can't steadily generated continuous electrical energy. Thus, the TRECs consist of n TREC, as shown in Fig. 1(a). It is assumed that the charging time is equal to the discharging time, the regenerative efficiency is equal to η_{R}. The TREC's *T-S* diagram is depicted in Fig. 1(b). In one cycle, a TREC is charged at a higher temperature T_{H} and then discharged at temperature T_{L} with higher voltage due to the opposite temperature coefficients of the two electrodes. Because the discharging voltage is larger than the charging voltage, net electricity

can be extracted from heat flow Q_{H} during the cycle. During the charging process, the chemical reactions taking palace in the positive and negative electrodes are listed as[13,14]

$$\begin{cases} \text{Positive electrode: } 2\mathrm{Na} \rightarrow 2\mathrm{Na}^{+} + 2e \\ \text{Positive electrode: } 2\mathrm{Na}^{+} + 2\mathrm{NO}_3^{-} \rightarrow 2\mathrm{NaNO}_3 \\ \text{Negative electrode: } \mathrm{Cu}\left(\mathrm{NO}_3\right)_2 \rightarrow \mathrm{Cu}^{+2} + 2\mathrm{NO}_3^{-} \\ \text{Negative electrode: } \mathrm{Cu}^{+2} + 2e \rightarrow \mathrm{Cu} \end{cases} \tag{6}$$

During the discharging process, the chemical reactions occurring in the two electrodes are listed as:

$$\begin{cases} \text{Positive electrode: } 2\mathrm{NaNO}_3 \rightarrow 2\mathrm{Na}^{+} + 2\mathrm{NO}_3^{-} \\ \text{Positive electrode: } 2\mathrm{Na}^{+} + 2e \rightarrow 2\mathrm{Na} \\ \text{Negative electrode: } \mathrm{Cu} \rightarrow \mathrm{Cu}^{+2} + 2e \\ \text{Negative electrode: } \mathrm{Cu}^{+2} + 2\mathrm{NO}_3^{-} \rightarrow \mathrm{Cu}\left(\mathrm{NO}_3\right)_2 \end{cases} \tag{7}$$

According to electrochemistry and heat transport, the heat flows absorbed from the PSC in the charging process and released to the environment in discharging process are, respectively, given by[13-15,20,22]

$$Q_{\mathrm{H}} = \alpha T_{\mathrm{H}} I_{\mathrm{T}} - I_{\mathrm{T}}^2 R_{\mathrm{I}} + \frac{C_{\mathrm{p}}}{C_{\mathrm{q}}} I_{\mathrm{T}} \left(T_{\mathrm{H}} - T_{\mathrm{L}}\right)\left(1-\eta_{\mathrm{R}}\right) \tag{8}$$

and

$$Q_{\mathrm{L}} = \alpha T_{\mathrm{L}} I_{\mathrm{T}} + I_{\mathrm{T}}^2 R_{\mathrm{I}} + \frac{C_{\mathrm{p}}}{C_{\mathrm{q}}} I_{\mathrm{T}} \left(T_{\mathrm{H}} - T_{\mathrm{L}}\right)\left(1-\eta_{\mathrm{R}}\right) \tag{9}$$

where α is isothermal coefficient. I_{T} is the operating current. R_{I} is internal resistance of electrode. $\alpha T_{\mathrm{H}} I_{\mathrm{T}}$ is rate of the heat that is provided by the PSC. $\alpha T_{\mathrm{L}} I_{\mathrm{T}}$ is the rate of the heat that is released into environment. $I_{\mathrm{T}}^2 R_{\mathrm{I}}$ is the Joule heat loss. $\frac{C_{\mathrm{p}}}{C_{\mathrm{q}}} I_{\mathrm{T}} \left(T_{\mathrm{H}} - T_{\mathrm{L}}\right)\left(1-\eta_{\mathrm{R}}\right)$ is the regenerative losses. C_{p} is the specific heat capacity. C_{q} is the specific charge capacity. η_{R} is the regenerative efficiency.

By using Eqs. (8) and (9), the generated power P_{T} from TRECs can be expressed as[13-15,20,22]

$$P_{\mathrm{T}} = m\left(Q_{\mathrm{H}} - Q_{\mathrm{L}}\right) = V_{\mathrm{T}} I_{\mathrm{T}}, \tag{10}$$

where $V_{\mathrm{T}} = m\left[\alpha\left(T_{\mathrm{H}} - T_{\mathrm{L}}\right) - 2I_{\mathrm{T}}R_{\mathrm{I}}\right]$ is the output voltage. m is the simultaneously charged number. It can be seen in Eq. 7, the power generation and efficiency of the TRECs depend on the internal resistance R_{I}, the temperatures T_{H} and T_{L}, and the isothermal temperature coefficient α.

2.3 | The overall electricity generation and efficiency of the system

The two subsystems are coupled through the energy balance equation. According to the energy balance analysis, the heat flow Q_{H} transferred from the PSC to the TREC can be denoted as

$$GA_{\mathrm{P}} - V_{\mathrm{P}} J_{\mathrm{P}} A_{\mathrm{P}} - UA_{\mathrm{P}}\left(T_{\mathrm{P}} - T_{\mathrm{E}}\right) = Q_{\mathrm{H}}, \tag{11}$$

where $U = 5\,\mathrm{W}\cdot\mathrm{m}^{-2}\cdot\mathrm{K}^{-1}$ is the natural convection heat transfer coefficient.

Inserting Eq. (8) into (11), a new energy balance equation is derived as

$$\left[G - V_{\mathrm{P}} J_{\mathrm{P}} - U\left(T_{\mathrm{P}} - T_{\mathrm{E}}\right)\right] A_{\mathrm{P}} = m\left[I_{\mathrm{T}}\alpha T_{\mathrm{H}} - I_{\mathrm{T}}^2 R_{\mathrm{I}} + \frac{C_{\mathrm{p}}}{C_{\mathrm{q}}} I_{\mathrm{T}}\left(T_{\mathrm{H}} - T_{\mathrm{L}}\right)\left(1 - \eta_{\mathrm{R}}\right)\right]. \tag{12}$$

Using Eqs. (5) and (10), the overall electricity generation P and the efficiency η of the system can be expressed as

$$P = P_{\mathrm{PSC}} + P_{\mathrm{T}} = V_{\mathrm{P}} J_{\mathrm{P}} A_{\mathrm{P}} + V_{\mathrm{T}} I_{\mathrm{T}} \tag{13}$$

and

$$\eta = \frac{P_{\mathrm{PSC}} + P_{\mathrm{T}}}{GA_{\mathrm{P}}} = \frac{V_{\mathrm{P}} J_{\mathrm{P}} A_{\mathrm{P}} + V_{\mathrm{T}} I_{\mathrm{T}}}{GA_{\mathrm{P}}}. \tag{14}$$

When the related parameters V_{P} of the PSC and V_{T} of the TRECs are given, J_{P}, T_{P}, and I_{T} can be calculated by solving Eq. (12). Inserting V_{P}, V_{T}, J_{P}, T_{P}, and I_{T} into Eqs. (13) and (14), one can calculate the power P and the efficiency η. Through numerical simulation and parametric analysis, the optimum performances of four different operating states will be studied in the next sections.

3 | COUPLED AND OPTIMIZED PROPERTIES

3.1 | Model validations

Considering the radiative recombination in PSC and the photons absorption from the environment, the expression for the dark current density J_r can be given by

$$J_r = J_{01} - J_{02} = q\int_0^{\lambda_g} \frac{2\pi hc^2}{\lambda^5} \left\{ \frac{1-\exp\left[-2a(\lambda)d\right]}{\exp\left[\left(hc/\lambda - qV_P\right)/\left(k_B T_P\right)\right]-1} - \frac{1-\exp\left[-2a(\lambda)d\right]}{\exp\left[hc/\left(\lambda k_B T_E\right)\right]-1} \right\} d\lambda . \quad (15)$$

The approximation $1/\left\{\exp\left[hc/\left(\lambda k_B T\right)\right]-1\right\} \approx 1/\exp\left[hc/\left(\lambda k_B T\right)\right]$ in Eq. (1) leads that the theoretical prediction values is larger than the experimental values in certain regions, as verified in Fig. 2(a). Fig. 2(b) demonstrates that the theoretical curve $V_T \sim \left(T_H - T_L\right)$ is close to the experimental curve. Therefore, the established PSC-TREC energy cascade utilization system in present work is valid.

3.2 | Performance analysis of the pure PSC

As the TRECs' electrical circuit is opened, it doesn't generate electricity. In such a case, the PSC releases low-grade thermal energy into the environment through convection heat transfer. The open-circuit voltage $V_{T,OC}$ is equal to $m\alpha\left(T_H - T_L\right)$. Inserting $I_T = 0$ into Eq. (12), the PSC's temperature T_P can be determined by numerical simulation. Based on the assumption $T_H = T_P$, the open-circuit $V_{T,OC} = m\alpha\left(T_H - T_L\right)$ can be obtained, which is called the electromotive force ε_T of TRECs. Thus, the curves of $V_{T,OC}$ and T_P as a function of V_P is illustrated in Fig. 3(a). In Fig. 3(a), the temperature T_P decreases first and then increases by increasing V_P, the variation tendency of open-circuit voltage is similar with the PSC's temperature T_P. By using Eqs. (1)-(4), (12), and (14), the dependences of efficiency η_P and current density J_P on V_P is plotted in Fig. 3(b), where $V_{P,OC}$ is the open-circuit voltage of the PSC. As $r_s \to 0$ and $r_{sh} \to \infty$, the open-circuit voltage $V_{P,OC}$ is approximately determined as

$$V_{\mathrm{P,OC}} = \frac{k_{\mathrm{B}} T_{\mathrm{P}}}{q} \ln\left(\frac{J_{\mathrm{ph}}}{J_0} + 1 \right). \tag{16}$$

It is seen from Fig. 3(b) that a maximum efficiency $\eta_{\mathrm{P,max}} = 0.183$ can be achieved when V_{P} and J_{P} are equal to $V_{\mathrm{P},\eta}$ and $J_{\mathrm{P},\eta}$, respectively. Combining Figs. 3(a) and 3(b), one can find that T_{P} achieves a minimum value $T_{\mathrm{P,min}}$ under the conditions $V_{\mathrm{P}} = V_{\mathrm{P},\eta}$ and $J_{\mathrm{P}} = J_{\mathrm{P},\eta}$.

3.3 | Performance analysis of the pure TRECs

As the PSC's circuit is opened, it can't produce power and only works as a heat source to drive the TRECs. In such a condition, the TREC's efficiency is denoted as η_{T}. The dependences of $V_{\mathrm{P,OC}}$ and T_{P} on V_{T} is shown in Fig. 4(a). Because of $T_{\mathrm{H}} = T_{\mathrm{P}}$ and $V_{\mathrm{T}} = m\left[\alpha \left(T_{\mathrm{H}} - T_{\mathrm{L}} \right) - 2 I_{\mathrm{T}} R_{\mathrm{I}} \right]$, the increase of TRECs' output voltage V_{T} depends on the increase of PSC's temperature T_{P}, while the increase of T_{P} leads to a decrease in $V_{\mathrm{P,OC}}$ with increasing V_{T}, as shown in Fig. 4(a). By using Eqs. (8)-(14), the dependences of efficiency η_{T} and electrical current I_{T} on V_{T} is plotted in Fig. 4(b). As depicted in Fig. 3(b), it can be approximately considered that I_{T} decreases linearly with the increase of V_{T}. As $V_{\mathrm{T}} = 0$ is set, the short-circuit electrical current $I_{\mathrm{T,SC}}$ can be determined as

$$I_{\mathrm{T,SC}} = \left[\alpha \left(T_{\mathrm{H}} - T_{\mathrm{L}} \right) \right] / \left(2 R_{\mathrm{I}} \right). \tag{15}$$

Further, Fig. 4(b) shows that a maximum efficiency $\eta_{\mathrm{T,max}} = 0.0337$ can be obtained when V_{T} and I_{T} are equal to $V_{\mathrm{T},\eta}$ and $I_{\mathrm{T},\eta}$, respectively.

3.4 | Coupled and optimized properties of the PSC-TREC tandem cells

When the tandem PSC-TREC is formed, the equivalent circuit is characterized to Fig. 5(a). The constraint relation between current I and voltage V is rewritten as[7]

$$I = I_{\mathrm{ph}} - I_0 \left\{ \exp\left[\frac{q(V + I(R_{\mathrm{s}} + R_{\mathrm{I}}) - \varepsilon_{\mathrm{T}})}{k_{\mathrm{B}} T_{\mathrm{P}}} \right] - 1 \right\} - \frac{V + I(R_{\mathrm{s}} + R_{\mathrm{I}}) - \varepsilon_{\mathrm{T}}}{R_{\mathrm{sh}}}, \tag{16}$$

where V and I are the net output voltage and current, respectively. $I_{ph} = J_{ph} A_P$ is the photo-generation current. $I_0 = J_0 A_P$ is the reverse saturation current of the diode. $R_s = r_s / A_p$ and $R_{sh} = r_{sh} / A_p$ are the serried and parallel resistances, respectively. The TREC's electromotive force is caudated as: $\varepsilon_T = V_{T,OC} = \alpha (T_H - T_L)$. For given three values of A_p, the curves of tandem cells' current I, the power output $P = VI$, and the efficiency η as a function of voltage V are presented in Fig. 4. Like the reported literatures,[7,10] the *I-V* curves of tandem cells mainly depends on that of the PSC, as demonstrated in Fig. 5(b). Figs. 5(b) and (c) show that the short-current I_{sh} and power output P are increased by increasing A_p, the open-circuit voltage V_{OC} changes small as A_p increases, while the efficiency η is decreased by increasing A_p. It should be pointed that although increasing the PSC's front surface area A_p can improve the power output P, the development large-scale PSC is challenging. Further, the low-cost, long-life, high-stability are also the key issues in the field of solar cells.

3.5 | Coupled and optimized properties of the coupled system

The above discussion reveal the dependences of the temperature T_P with V_P and V_T, which can be verified in Fig. 6(a). The PSC's voltage-current characteristic leads to monotonical decrease of electrical current I_P with increasing V_P, as demonstrated in Fig. 6(b). Because the positive correlation $V_T \sim T_P$ and negative correlation $I_P \sim T_P$, I_P monotonically decreases by increasing V_T, as proven in Fig. 6(b). Fig. 6(c) shows that the electrical current I_T is a monotonically decreasing function of V_T as V_P is fixed, which is determined by the TRECs' voltage-current characteristics. Fig. 6(c) displays that V_P can be optimized to obtain a local minimum current $I_{T,min}$ as V_T is fixed, the phenomenon is determined as the correlation $V_P \sim T_P$. Fig. 6(d) reveals that there exist optimal values

$V_{\mathrm{P},\eta}$ and $V_{\mathrm{T},\eta}$ at which the efficiency attains its optimal value $\eta_{\max}$. Based on the optimal values $V_{\mathrm{P},\eta}$ and $V_{\mathrm{T},\eta}$, one can calculate the optimal values $T_{\mathrm{P},\eta}$, $I_{\mathrm{P},\eta}$, and $I_{\mathrm{T},\eta}$. Thus, the coupled system's optimal performance can be achieved by adjusting the thermal and the electrical parameters. It is should be pointed that the parametric optimal values depend on the structure parameter d. In next section, the dependence of d on the overall maximum efficiency and operating conditions will be revealed.

The dependences of photo-generation current density J_{ph} on thickness d is obtained from Ref. [17]. At a given d, the maximum efficiency $\eta_{\max}$ and the optimal values $T_{\mathrm{P},\eta}$, $V_{\mathrm{P},\eta}$, and $V_{\mathrm{T},\eta}$ can be calculated based on the values of J_{ph}. Thus, the curves of $\eta_{\max}$ and $T_{\mathrm{P},\eta}$ as a function of d is plotted in Fig. 7(a). It is seen from Fig. 7(a) that one can select an optimum $d_{\mathrm{M}} = 484\,\mathrm{nm}$ to obtain an overall maximum efficiency $\eta_{\mathrm{M}} = 0.249$. Obviously, η_{M} determines the coupled system's performance limit. Fig. 7(a) displays that the variation of $T_{\mathrm{P},\eta}$ with d and the variation of $\eta_{\max}$ with d are opposite. Fig. 7(b) shows that the variation of $V_{\mathrm{P},\eta}$ with d is similar with the variation of $V_{\mathrm{T},\eta}$ with d. By using optimum value d_{M}, the optimum temperature $T_{\mathrm{P,M}} = 371\mathrm{K}$, voltages $V_{\mathrm{P,M}}$=0.963 V and $V_{\mathrm{T,M}}$=0.0597 V, electrical currents $I_{\mathrm{P,M}}$=0.412 A and $I_{\mathrm{T,M}}$=0.869 A can be determined. According to $V_{\mathrm{P,M}}$, $V_{\mathrm{T,M}}$, $I_{\mathrm{P,M}}$, $I_{\mathrm{T,M}}$, the load resistances $R_{\mathrm{L1,M}} = 2.34\,\Omega$ and $R_{\mathrm{L2,M}} = 0.0988\,\Omega$ can be matched. From analyses above, one can find that the optimum value $R_{\mathrm{L2,M}}$ is very small. For the sake of the enhancement of the load-driven performance, the number of TREC in series should be increased. The results can supply a strategy to obtain optimum performances of the PSC-TREC coupled system through load matching.

Comparing Fig. 7 to Figs. 2, 3, 4, and 5, one can discover that the performance of the PSC-TRECs is superior to those of the pure PSC, pure TREC, and PSC-TRECs tandem cells. The results reveal that

emission of the waste heat from the PSC can be well utilized, and the solar energy utilization can be improved.

3.6 | The effects of key factors on the optimum performances

In the above analysis, the PSC's front surface area is fixed, and the non-radiative recombination losses (NRLs) are neglected. In this section, we will discuss the effects of the PSC's front surface area and the NRLs on the optimum performances. When the NRLs such as Auger and Shockley-Read-Hall (SRH) are considered, the relationship between the non-ideal current density J_{P} and operating voltage V_{P} is revised as[4]

$$J_{\mathrm{P}} = J_{\mathrm{ph}} - J_{\mathrm{Auger}} - J_{\mathrm{SRH}} - J_0 \left\{ \exp\left[\frac{q\left(J_{\mathrm{PV}} r_{\mathrm{s}} + V_{\mathrm{P}}\right)}{k_{\mathrm{B}} T_{\mathrm{P}}} \right] - 1 \right\} - \frac{V_{\mathrm{P}} + J_{\mathrm{P}} r_{\mathrm{s}}}{r_{\mathrm{sh}}}, \tag{17}$$

where the Auger current density loss J_{Auger} and the SRH current density loss J_{SRH} are expressed as[4]

$$J_{\mathrm{Auger}} = q\gamma_{\mathrm{Auger}} N_{\mathrm{i}}^3 d \exp\left[\frac{3qV_{\mathrm{P}}}{2k_{\mathrm{B}} T_{\mathrm{P}}} \right] \tag{18}$$

and

$$J_{\mathrm{SRH}} = \frac{qN_{\mathrm{i}} d}{\tau_{\mathrm{SRH}}} \exp\left(\frac{qV_{\mathrm{P}}}{2k_{\mathrm{B}} T_{\mathrm{P}}} \right), \tag{19}$$

where $\gamma_{\mathrm{Auger}} = 1.1\times10^{-40}\ \mathrm{m^6\cdot s^{-1}}$ is the Auger recombination coefficient.[4] $\tau_{\mathrm{SRH}} = 100\,\mu\mathrm{s}$ is the SRH recombination time.[31] N_{i} is the intrinsic concentration, which can be calculated as

$$N_{\mathrm{i}} = \sqrt{N_{\mathrm{c}} N_{\mathrm{v}}} \left(\frac{T_{\mathrm{P}}}{300} \right)^{1.5} \exp\left(\frac{-E_{\mathrm{g}}}{2k_{\mathrm{B}} T_{\mathrm{P}}} \right), \tag{20}$$

where $N_{\mathrm{c}} = 3.97\times10^{24}\ \mathrm{m^{-3}}$ and $N_{\mathrm{v}} = 3.97\times10^{24}\ \mathrm{m^{-3}}$ are the state densities of the conduction and the valence at 300 K, respectively.[28]

For given three different values of A_{p}, the overall maximum efficiencies and the corresponding conditions in absence (case1) and presence (case 2) of the NRLs are listed in Table 2. It is observed

from Table 2 that the NRLs have obvious influence on d_{M}, while they have negligible impacts on other parametric conditions and the overall maximum efficiency. The results indicate that the impacts of the NRLs on the overall maximum efficiency of the coupled system can be mitigated by adjusting the thickness d. Table 2 shows that A_{P} has small influence on d_{M}, while the decreasing of A_{P} can increase η_{M} and $V_{\mathrm{P,M}}$, and reduce $V_{\mathrm{T,M}}$, $I_{\mathrm{P,M}}$, $I_{\mathrm{T,M}}$, and $T_{\mathrm{P,M}}$. Because the electricity mainly comes from the PSC, the input solar energy is decreased with decreasing of A_{P}, which leads to a reduction in the temperature T_{P}, as determined by the energy balance Eq. (12). The correlations $J_{\mathrm{P}} \sim T_{\mathrm{P}}$ and $V_{\mathrm{P}} \sim T_{\mathrm{P}}$ determine the improvement of P_{PSC}, and thus, the overall P and η increase.

Performances comparisons demonstrate that all the maximum efficiencies in Table 2 are superior to the maximum efficiency 25% in recent work[32], and thus, the TREC is more suitable for waste heat recovery of PSCs than the TEM.

4 | CONCLUSIONS

A conceptual model of the PSC-TREC system has been established. The main conclusions are summarized as follows:

(1) The maximum efficiency and the related parametric characteristics of the three typical operating states are studied and compared. As the TREC works is opened, the maximum efficiency $\eta_{\mathrm{P,max}} = 0.183$ of the single PSC can be achieved. As the PSC is opened, the maximum efficiency of the pure TREC $\eta_{\mathrm{T,max}} = 0.0337$ can be presented. In addition, the maximum efficiency the PSC-TREC tandem cells can be adjusted by designing different A_{P}.

(2) The thermal and electrical properties of the independent PSC and TREC are revealed. For given $A_{\mathrm{P}} = 1.8 \times 10^{-3}\ \mathrm{m}^2$, the maximum efficiency $\eta_{\max}$=0.249 and the corresponding optimum conditions

$d_{\mathrm{M}} = 484\,\mathrm{nm}$, $T_{\mathrm{P,M}} = 371\mathrm{K}$, $V_{\mathrm{P,M}}$=0.963 V , $V_{\mathrm{T,M}}$=0.0597 V , $I_{\mathrm{P,M}}$=0.412 A , $I_{\mathrm{T,M}}$=0.869 A , $R_{\mathrm{L1,M}} = 2.34\ \Omega$, and $R_{\mathrm{L2,M}} = 0.0988\ \Omega$ are obtained.

(3) The impacts of the NRLs on the optimum performances of the coupled system can be mitigated according to adjust the structure parameter d. Moreover, the design of the PSC's front surface area A_{p} is of great importance for the operation of coupled system.

The results obtained can offer guidance for the optimal design of actual systems and the efficient utilization of solar energy.

ACKNOWLEDGEMENTS

This work has been supported by the Chongqing Research Program of Basic Research and Frontier Technology (cstc2020jcyjmsxmX0001), the Science and Technology Research Program of Chongqing Municipal Education Commission (Grant No. KJQN201901144) and Scientific Research Foundation of Chongqing University of Technology (Grant No. 2019ZD22), People's Republic of China. M. NI also thanks the financial support by Hong Kong Polytechnic University (Project ID: P0014036, account: G-YW3T) and grants (Project Number: PolyU 152214/17E and PolyU 152064/18E) from Research Grant Council, University Grants Committee, Hong Kong SAR.

DATA AVAILABILITY

Data sharing is not applicable to this article as no new data were created or analyzed in this study.

REFERENCES

1. Domanski K, Alharbi E A, Hagfeldt A, *et al.* Systematic investigation of the impact of operation conditions on the degradation behaviour of perovskite solar cells. Nat. Energy 2018; 3: 61–67.

2. Wang M, Chamberland N, Breau L, *et al.* An organic redox electrolyte to rival triiodide/iodide in dye-sensitized solar cells. Nat. Chem. 2010; 2: 385–389.

3. Grätzel M. The light and shade of perovskite solar cells. Nat. Mater. 2014; 13: 838842.

4. Kim K, Lee S. Detailed balance analysis of plasmonic metamaterial perovskite solar cells. Opt. Express 2019; 27: A1241–A1260.

5. Kim D I, Lee J W, Jeong R H, Yang J W, Park S, Boo JH. Optical and water-repellent characteristics of an anti-reflection protection layer for perovskite solar cells fabricated in ambient air. Energy, 2020; 210: 118582.

6. Tress W, Domanski K, Carlsen B, Agarwalla A, Alharbi EA, Graetzel M, Hagfeldt A. Performance of perovskite solar cells under simulated temperature-illumination real-world operating conditions. Nat. Energy 2019; 4(7): 568–574.

7. Liao T, He Q, Xu Q, Dai Y, Cheng C, Ni M. Performance evaluation and optimization of a perovskite solar cell-thermoelectric generator hybrid system, Energy 2020; 201: 117665.

8. Xu L, Xiong Y, Mei A, Hu Y, Rong Y, Zhou Y, Hu B, Han H. Efficient Perovskite Photovoltaic-Thermoelectric Hybrid Device. Advanced Energy Materials 2018; 8: 1702937.

9. Fu P, Qin W, Bai S, Yang D, Chen L, Guo X, Li C. Integrating large-area perovskite solar module with thermoelectric generator for enhanced and stable power output. Nano Energy 2019; 65: 104009.

10. Zhou Y, Yin X, Zhang Q, Wang N, Yamamoto A, Koumoto K, Shen H, Lin H. Perovskite solar cell-thermoelectric tandem system with a high efficiency of over 23%. Materials Today Energy 2019; 12: 363–370.

11. Liu Z, Sun B, Zhong Y, Liu X, Han J, Shi T, Tang Z, Liao G. Novel integration of carbon counter electrode based perovskite solar cell with thermoelectric generator for efficient solar energy conversion. Nano Energy 2017; 38: 457–466.

12. Zhang J, Xuan Y, Yang L. A novel choice for the photovoltaic–thermoelectric hybrid system: the perovskite solar cell. Int. J. Energy Res. 2016; 40: 1400–1409.

13. Fathabadi H. Solar energy harvesting in buildings using a proposed novel electrochemical device as an alternative to PV modules. Renew. Energy 2019; 133: 118–125.

14. Fathabadi H. Improving the power Efficiency of a PV power generation system using a proposed electrochemical heat engine embedded in the system. IEEE Transac. Power Electronics 2019; 34: 0885–8993.

15. Zhao Q, Guo X, Zhang H, Ni M, Hou S. Performance evaluation of a novel photovoltaic-electrochemic hybrid system. Energy Convers. Manage 2019; 195: 1227–1237.

16. Guo J, Wang Y, Gonzalez-Ayala J, *et al.* Continuous power output criteria and optimum operation strategies of an upgraded thermally regenerative electrochemical cycles system. Energy Convers. Manage., 2019; 180: 654-664.

17. Lee S W, Yang Y, Lee H W, Ghasemi H, Kraemer D, Chen G, *et al.* An electrochemical system for efficiently harvesting low-grade heat energy. Nat. Commun. 2014; 5: 3942.

18. Yang Y, Loomis J, Ghasemi H, Lee S W, Wang Y J, Cui Y, *et al*. Membrane free battery for harvesting low-grade thermal energy. Nano Lett. 2014; 14: 6578–6583.

19. Yang Y, Lee S W, Ghasemi H, Loomis J, Li X, Kraemer D, et al. Charging-free electrochemical system for harvesting low-grade thermal energy. Proc. Natl. Acad. Sci. U.S.A. 2014; 111: 17011–17016.

20. Wang Y, Cai L, Peng W, Zhou Y, Chen J. Maximal continuous power output and parametric optimum design of an electrochemical system driven by lowgrade heat. Energy Convers. Manag. 2017; 138: 156–161.

21. Ding Y, Guo X, Ramirez-Meyers K, Zhou Y, Zhang L, Zhao F, Yu G. Simultaneous energy harvesting and storage via solar-driven regenerative electrochemical cycles. Energy Environ. Sci. 2019; 12: 3370–3379.

22. Zhang X, Cai L, Liao T, Zhou Y, Zhao Y, J. Chen, Exploiting the waste heat from an alkaline fuel cell via electrochemical cycles. Energy 2018; 142: 983–990.

23. Guo X, Zhang H. Performance analyses of a combined system consisting of high-temperature polymer electrolyte membrane fuel cells and thermally regenerative electrochemical cycles. Energy 2019; 13: 116720.

24. Zhou Y, Chen Y, Zhang Q, *et al.* A highly-efficient concentrated perovskite solar cell-thermoelectric generator tandem system. J. Energy Chemistry, 2021; 59: 730−735.

25. Xu T, Wang Z, Li X, Sha W, Loss mechanism analyses of perovskite solar cells with equivalent circuit model. Acta Phys. Sin. 2021; 70(9): 098801.

26. Zaky A A, Ibrahim M N, Rezk H, et al. Energy efficiency improvement of water pumping system using synchronous reluctance motor fed by perovskite solar cells. Int. J. Energy Research, 2020, 44(14): 11629–11642.

27. Zhang L, Ding S, Qin G. Efficiency simulations on perovskite solar cells only using experimentally determined reflectance and transmittance data. Sol. Energy Mater. Sol. Cells 2019; 201: 110039.

28. Nemnes G A, Besleaga C, Tomulescu A G, Pintilie I, Pintilie L, Torfason K, Manolescu A. Dynamic electrical behavior of halide perovskite based solar cells. Sol. Energy Mater. Sol. Cells 2017; 159: 197–203.

29. Nkele AC, Nwanya AC, Shinde NM, et al. The use of nickel oxide as a hole transport material in perovskite solar cell configuration: achieving a high performance and stable device. Int.. J. Energy. Res. 2020; 44(13): 9839–9863..

30. Sha W E I, Ren X, Chen L, Choy W C H. The efficiency limit of $CH_3NH_3PbI_3$ perovskite solar cells. Appl. Phys. Lett. 2015; 106: 221104.

31. Pazos-Outón L M, Patrick Xiao T, Yablonovitch E. Fundamental Efficiency Limit of Lead Iodide Perovskite Solar Cells. J. Phys. Chem. Lett. 2018; 9: 1703−1711.

32. Cheng C, Wang S, Tan P, *et al*. Insights into the thermopower of thermally regenerative electrochemical cycle for low grade heat harvesting. ACS Energy Lett., 2020; 6: 329−336.

List of Figures and Tables

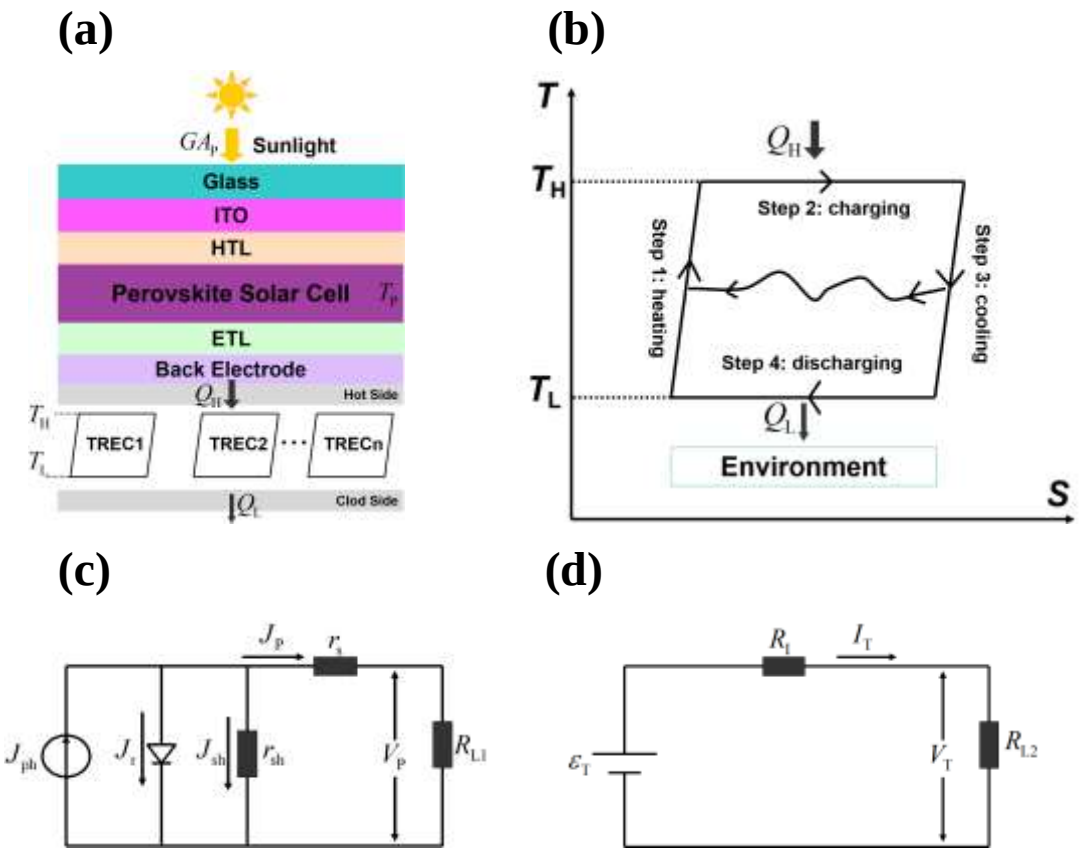

Figure 1 (a) the schematic diagram of a PSC-TREC coupled system, (b) temperature-entropy diagram, (c) the equivalent circuit of a PSC, and (d) the equivalent circuit of a TREC.

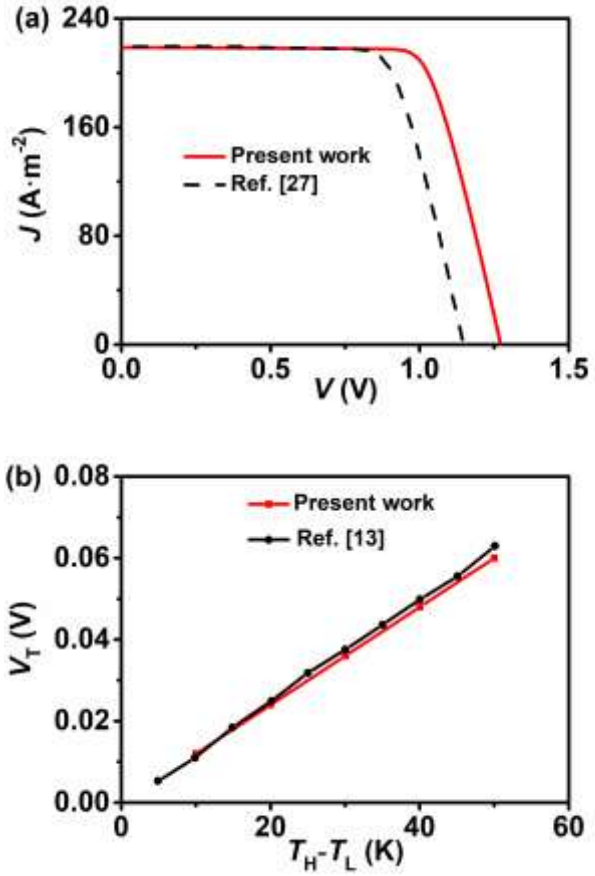

Figure 2 The model validations for the PSC and the TRECs.

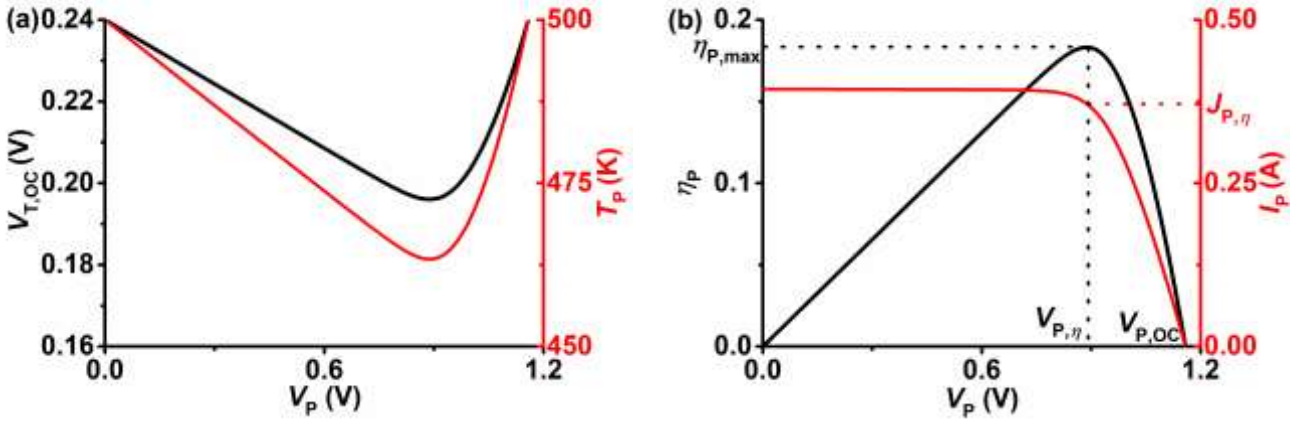

Figure 3 The curves of (a) the TRECs' open-circuit voltage $V_{\mathrm{T,OC}}=\alpha\left(T_{\mathrm{H}}-T_{\mathrm{L}}\right)$ and the PSC's temperature T_{P} and (b) the PSC's efficiency η_{P} and the electrical current I_{P} varying with the output voltage V_{P}, where the parameters $m=1$, $n=2$, $G=1000\,\mathrm{W\cdot m^{-2}}$, $T_{\mathrm{L}}=T_{\mathrm{E}}=300\,\mathrm{K}$, $d=200\,\mathrm{nm}$, $A_{\mathrm{p}}=1.8\times10^{-3}\,\mathrm{m^2}$ are chosen.

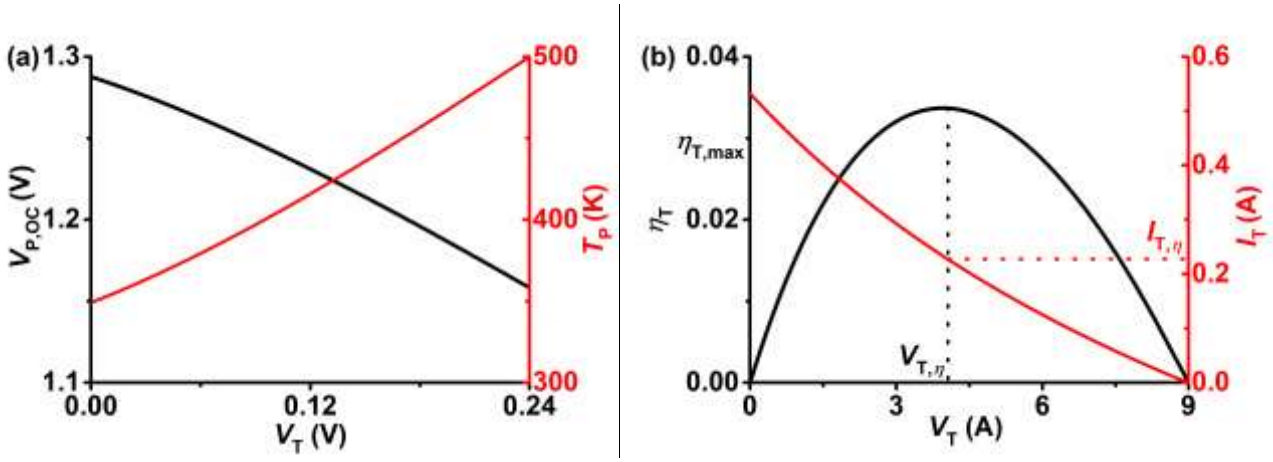

Figure 4 The curves of (a) the PSC's open-circuit voltage $V_{P,OC}$ and the PSC's temperature T_P and (b) the TRECs' efficiency η_T and the electrical current I_T varying with the output voltage V_T, where the values of the parameters are same as Fig. 2.

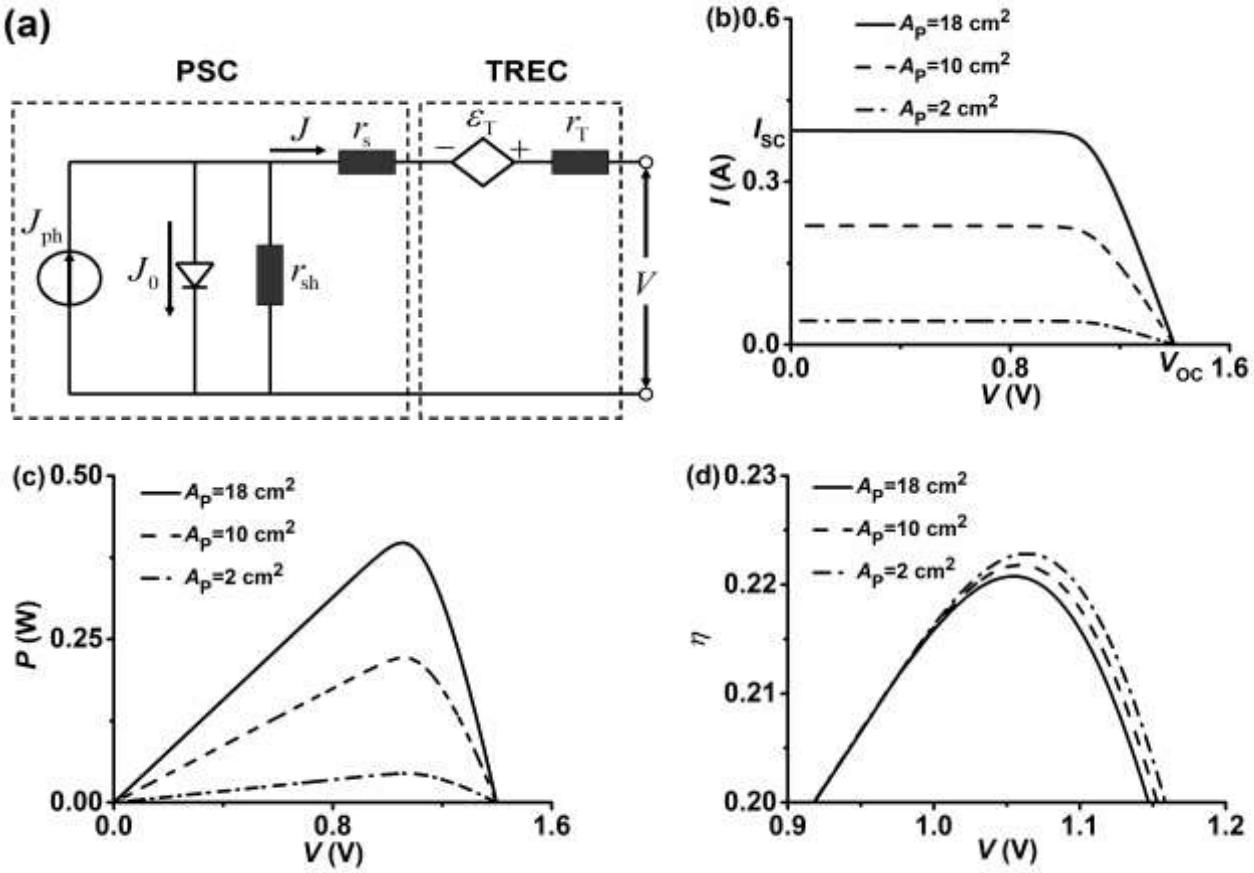

Figure 5 (a) The equivalent circuit of the PSC-TREC tandem cells, (b) the voltage-current characteristics curves of the tandem cells, (c) the curves of the power output P and (d) the efficiency of the tandem cells as a function of the total output voltage V .

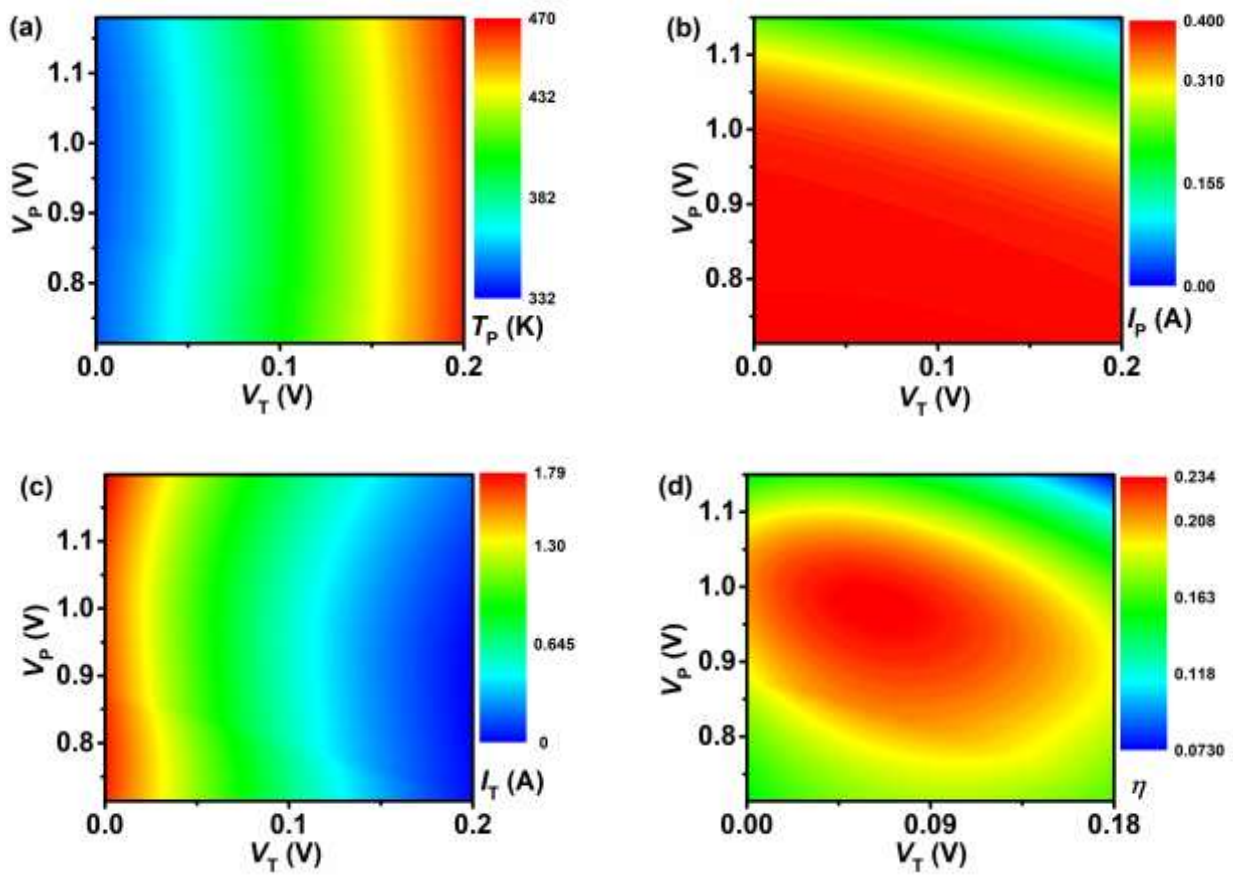

Figure 6 The three-dimensional projection graphs of (a) the PSC's temperature T_P of, (b) the PSC's electrical current density I_P the PSC, (c) the TREC's electrical current density I_T the PSC, and (d) the efficiency η of the coupled system varying with variables V_P and V_T, where the values of the parameters are same as Fig. 2.

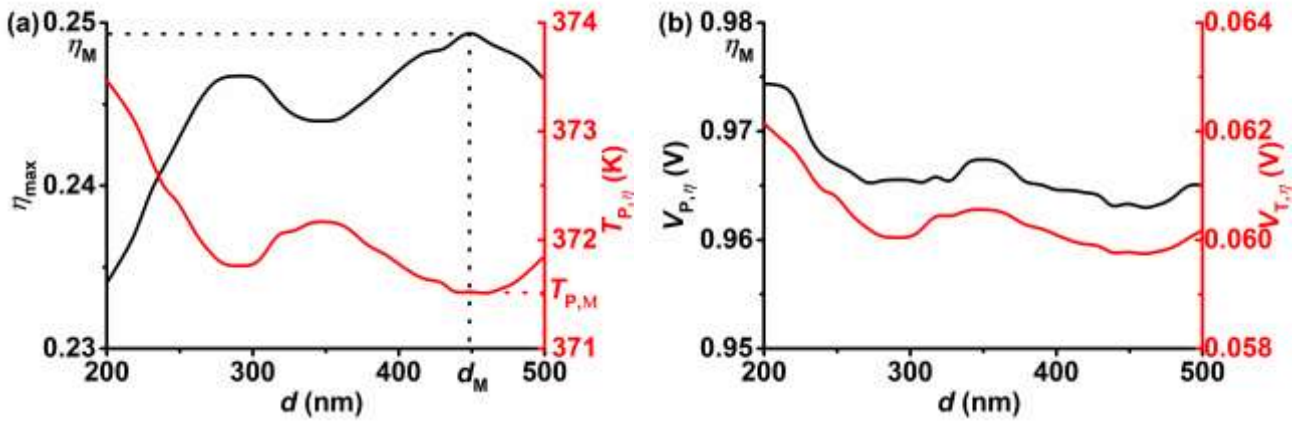

Figure 7 The curves of (a) the maximum efficiency $\eta_{\max}$ and the optimum temperature $T_{\mathrm{P},\eta}$ and (b) the optimum voltages $V_{\mathrm{P},\eta}$ and $V_{\mathrm{T},\eta}$ at $\eta_{\max}$ as a function of d.

TABLE 1 the parametric selection of the TREC.[22]

Parameters	Value
Isothermal temperature coefficient, $\alpha\left(\mathrm{V}\cdot\mathrm{K}^{-1}\right)$	1.2×10^{-3}
Environment temperature, $T_{\mathrm{E}}\left(\mathrm{K}\right)$	300
Internal resistance of each electrode, $R_{\mathrm{I}}\left(\Omega\right)$	0.015
Specific heat capacity, $C_{\mathrm{p}}\left(\mathrm{J}\cdot\mathrm{K}^{-1}\cdot\mathrm{kg}^{-1}\right)$	2.408
Specific charge capacity, $C_{\mathrm{q}}\left(\mathrm{A}\cdot\mathrm{h}\cdot\mathrm{kg}^{-1}\right)$	32.43
Regenerative efficiency, η_{R}	0.70

TABLE 2 The effects of PSC's front surface area and carrier non-radiative recombination losses on overall efficiency and operating conditions.

$A_{\mathrm{P}}\left(\mathrm{cm}^2\right)$	Cases	η_{M}	$V_{\mathrm{P,M}}\left(\mathrm{V}\right)$	$V_{\mathrm{T,M}}\left(\mathrm{V}\right)$	$I_{\mathrm{P,M}}\left(\mathrm{A}\right)$	$I_{\mathrm{T,M}}\left(\mathrm{A}\right)$	$T_{\mathrm{P,M}}\left(\mathrm{K}\right)$	$d_{\mathrm{M}}\left(\mathrm{nm}\right)$
18	1	0.249	0.963	0.0597	0.412	0.869	371	484
	2	0.249	0.962	0.0595	0.411	0.871	371	448
10	1	0.257	0.972	0.0566	0.229	0.581	362	484
	2	0.255	0.972	0.0563	0.229	0.583	362	448
2	1	0.266	0.988	0.0509	0.0460	0.157	346	484
	2	0.266	0.990	0.0496	0.0458	0.158	345	448